

GT2017-64609

Catalytic Influence of Water Vapor on Lean Blowoff and NO_x Reduction for Pressurized Swirling Syngas Flames

Daniel Pugh * Philip Bowen Andrew Crayford Richard Marsh †
Jon Runyon † Steven Morris Anthony Giles

Cardiff School of Engineering,
Cardiff University, Wales, UK.

Email: pughdg@cardiff.ac.uk;
Tel. +44(0) 2920 870597

ABSTRACT

It has become increasingly cost-effective for the steel industry to invest in the capture of heavily carbonaceous BOF (Basic Oxygen Furnace) or converter gas, and use it to support the intensive energy demands of the integrated facility, or for surplus energy conversion in power plants. As industry strives for greater efficiency via ever more complex technologies, increased attention is being paid to investigate the complex behavior of by-product syngases. Recent studies have described and evidenced the enhancement of fundamental combustion parameters such as laminar flame speed due to the catalytic influence of H₂O on heavily carbonaceous syngas mixtures. Direct formation of CO₂ from CO is slow due to its high activation energy, and the presence of disassociated radical hydrogen facilitates chain branching species (such as OH), changing the dominant path for oxidation. The observed catalytic effect is non-monotonic, with the reduction in flame temperature eventually prevailing, and overall reaction rate quenched. The potential benefits of changes in water loading are explored in terms of delayed lean blowoff, and primary emission reduction in a premixed turbulent swirling flame, scaled for practical relevance at conditions of elevated temperature (423 K) and pressure (0.1-0.3 MPa). Chemical kinetic models are used initially to characterize the influence that H₂O has on the burning characteristics of the fuel blend employed, modelling laminar flame speed and extinction strain rate across an experimental range with H₂O vapor fraction increased to eventually diminish the catalytic effect. These modelled predictions are used as a foundation to investigate the experimental flame. OH chemiluminescence and OH planar laser induced fluorescence (PLIF) are employed as optical diagnostic techniques to analyze changes in heat release structure resulting from the experimental variation in water loading. A comparison is made with a CH₄/air flame and changes in lean blow off stability limits are quantified, measuring the incremental increase in air flow and again compared against chemical models. The compound benefit of CO and NO_x reduction is quantified also, with production first decreasing due to the thermal effect of H₂O addition from a reduction in flame temperature, coupled with the potential for further reduction from the change in lean stability limit. Power law correlations have been derived for change in pressure, and equivalent water loading. Hence, the catalytic effect of H₂O on reaction pathways and reaction rate predicted and observed for laminar flames, are compared against the challenging environment of turbulent, swirl-stabilized flames at elevated temperature and pressure, characteristic of piratical systems.*

INTRODUCTION

Over the last decade the fraction of crude steel produced worldwide in oxygen blown converters has increased each year, ultimately accounting for 74% of the 1,668 million tonnes of produced steel in 2014 [1]. The decarburization process is achieved through the batched introduction of oxygen to carbon-saturated iron, and produces vast quantities of a gaseous by-product generally referred to as BOS, BOF (Basic Oxygen Steelmaking/Furnace), or converter gas. For every tonne of liquid steel produced, there is typically 350-700 MJ of chemical energy available in converter gas [2]. It has therefore become increasingly cost-effective for plants to invest in the capture of this by-product fuel, and use it to support the intensive energy demands of the integrated facility, or for surplus energy conversion in power plants. This enhances the importance of research into the behavior of by-product fuels as industry strives for the application of cleaner, more efficient processes and complex technologies.

* Address all correspondence to this author.

† ASME Member

Converter gas typically comprises 50-80% CO, 10-18% CO₂, 1-3% H₂ in a balance of N₂ (%mol) [2]. The influence of water on this increasingly utilized fuel is highly relevant in applied combustion [3-8], as it provides a potential dissociative catalytic influence on CO oxidation across a limited range: Direct formation of CO₂ from CO is slow due to a high activation energy, and the presence of hydrogen facilitates chain branching OH formation, altering the dominant path for oxidation [3-12]. Water addition therefore induces competition between dissociative catalytic enhancement in reaction rate, contrasted against a reduction in flame temperature. This provides a non-monotonic influence on premixed flame propagation, increasing laminar flame speed and reaction rate at lower concentrations, before eventually diluting and quenching the flame. Recent studies undertaken with a converter gas mixture demonstrated the potential for large increases in laminar flame speed - up to 70% - with the addition of water vapor, as concentrations varied by amounts representative of change in atmospheric humidity [4]. This level of fluctuation was shown to provide a significant impact on the behavior of a 100 kW swirling flame at atmospheric inlet conditions with vapor and a liquid spray, changing the lean stability limit and reducing NO_x emissions [8].

AIMS OF THIS WORK

The aim of the investigation was to appraise the effect of humidifying premixed reactant flow at elevated temperature, with resultant water fractions more representative of those employed in Humidified Air Turbine (HAT) cycles, and beyond the pinnacle of catalytic enhancement to converter gas flame behavior [8, 13]. The influence of increasing pressure was also investigated, to assess the potential for change in flame response from increased water loading concentrations [10-12]. Change in flame shape and structure were appraised using optical diagnostic techniques (OH* chemiluminescence and OH Planar Laser Induced Fluorescence (PLIF)), in addition to quantifying the change in lean blowoff behavior. The produced emissions are also quantified, with power law correlations derived for a change in pressure.

EXPERIMENTAL FACILITY

Experiments were undertaken using a premixed swirl burner, housed within the high pressure optical chamber at Cardiff University's Gas Turbine Research Centre (GTRC), modified from previous work [8]. Components of the burner and casing assembly are shown as a schematic in Fig. 1. An instrumentation lance (Fig. 1(a)) is fed through the burner centerline, facilitating in-flame pressure and temperature measurements. Preheated reactants enter the burner inlet plenum (Fig. 1(b)) with mass flowrates quantified using suitably scaled Coriolis meters (Emerson CMF025M \pm 0.35%). Pre-vaporized steam was supplied to the plenum using a 2.5 kW heated supply line (Winkler WAMX1537), with the burner conditioned to operational temperature using preheated air prior to light-up. Liquid water supply was regulated using another scaled mass flow controller (Bronkhorst mini CORI-FLOW (\pm 0.2%)) and vaporized in two heaters (Watlow CASTX - 4.5 kW) feeding the supply line. After entering the plenum, reactants travel through the premix chamber (Fig. 1(c)) to a single radial-tangential swirler (Fig. 1(d)) and out the burner exit nozzle (20 mm radius). The outlet has a geometric swirl number (ratio of tangential to axial momentum) equivalent to $Sg=0.8$ [14, 15]. Optical access is afforded via orthogonal quartz viewing windows (Fig. 1(e)) housed within the 1.6 MPa rated (at 900 K) pressure casing (Fig. 1(f)). Chemiluminescence and PLIF data were optically captured from above, with the planar beam delivered through the perpendicular side window. The burner was operated with a cylindrical quartz exhaust confinement tube, and at a fixed expansion ratio of 2.5 from the burner nozzle exit (Fig. 1(g)), reduced from 3.5 in previous work [8]. The exhaust was sampled downstream of the confinement, with further detail on the measurement techniques provided in subsequent sections. Several transducers were installed to monitor operational conditions that were influential to the experimental result: K-type thermocouples (\pm 2.2 K) were installed on the inlet lines and premix chamber to monitor the temperature of preheated reactants entering the system, in addition to the burner face, lance tip and exhaust exit. Static pressure transducers (Druck PDCR (\pm 0.04%)) were housed in the inlet plenum and casing to give the supplied differential pressure across the burner nozzle. Dynamic pressure transducers were also installed in the burner face, lance and exhaust to monitor the acoustic response of the system, however these data are not presented in this work. The system was pressurized using a water-cooled back-pressure valve with incremental control, and a bypass airline in the exhaust.

CHEMILUMINESCENCE

The chemiluminescence of an excited hydroxyl (OH) intermediate radical (wavelength \sim 310 nm) has been used to provide a non-intrusive qualitative indication of localized heat release, and a generalized marker of flame front location [16-18]. In these experiments the OH* signal was captured using a Dantec Hi Sense Mk II CCD camera with a 1.3 megapixel resolution, coupled to an (Hamamatsu C9546-03L) image intensifier. A 78 mm focal length UV lens (F-stop = $f/3.8$) was installed on the intensifier, together with a narrow band pass filter (300-330 nm). The image plane is centered on the burner exit, with respective view fields of \sim 100 mm and \sim 75 mm in the radial and axial directions, corresponding to a resolution of \sim 13.6 pix/mm. For each experiment, 200 images were captured at a rate of 10 Hz with timing controlled by commercial software and a gate pulse generator set at 400 μ s, triggered by the camera aperture signal. The gain of the image intensifier was held constant for all experiments. The intensities measured for the 200 image dataset were

background corrected and averaged, with a condition-normalized false colourmap (correlated to pixel relative signal intensity, min - max), to provide a visual representation of the flame structure and localized heat release.

The flow-field generated by the swirl configuration has been previously evaluated using particle image velocimetry [19], with a flame structure typical for a premixed swirler of this design [20]: The outward forward flow generates a conical flame around a shear layer of zero axial velocity, and central recirculation zone (CRZ). OH* chemiluminescence is captured line-of-sight, meaning the image includes light emitted both in front and behind the focal plane of the imaging system. In the case of swirl-stabilized flames evaluated herein, the resulting images show intensity from the three-dimensional, conical shape of the flame (Fig. 2(a) - figure is oriented so flow is from bottom to top, with intensities normalized to the image maximum). A modified open-access Abel inversion algorithm [21] was used to transform the 3-D images captured into 2-D planar representations of the OH* chemiluminescence intensity distribution, with the underlying assumption that the swirl-stabilized flame is axisymmetric about its centerline (Fig. 2(b)) [20-23]. Both chemiluminescence, and Abel deconvoluted images are presented for the undertaken experiments. Detailed information regarding the image capture system and processing technique can be found in other works [23].

PLANAR LASER INDUCED FLUORESCENCE

Qualitative planar laser induced fluorescence (PLIF) measurements were also obtained for each experimental condition. The PLIF system comprised a (Quantel TDL-90) dye laser pumped by the 532 nm output beam of a frequency-doubled (Spectra Physics GCR 170-10) Nd:YAG laser operating at 10 Hz. The output beam of the TDL-90 was tuned to 283 nm to excite the (1,0) band of the OH radical, with fluorescence captured at 315 nm using the same intensified CCD camera system as for the OH* chemiluminescence measurements. The output beam from the dye laser was then directed through a set of telescopic sheet-forming optics to provide a laser sheet 25 mm in width. The camera was focused on the burner nozzle centerline perpendicular to both the laser sheet and fluid flow. This system produces pulse energies of roughly 12 mJ/pulse at 283.01 nm. Given the short lifetime of the OH radical fluorescence signal and the influence of quenching effects, the gate timing of the image intensifier was set to 100 ns, triggered by the Q-switch of the Nd:YAG laser to ensure that signal capture was appropriately timed with the laser excitation light pulse. The image intensifier gain was held constant for all experiments to ensure comparability, while reducing signal to noise ratio as much as possible. 500 images were taken for each condition at a rate of 10 Hz, with the same approximate view fields and pixel resolution as the OH* chemiluminescence images. The obtained image intensities were again temporally averaged, and corrected for background reflected light. The uncertainties in obtaining quantitative PLIF measurements are significant, with correction required for changes in collisional quenching, temperature, and pressure [24] for each condition. Qualitative results were therefore analyzed for the relative change in normalized OH concentration profiles as markers for OH distribution and compared against the profiles given by the models, similar to other equivalent works [20, 25].

EXHAUST EMISSION MEASUREMENTS

The exhaust stream was sampled using a multi-point equal area probe (7 holes) located within one equivalent diameter of the quartz confinement tube in accordance with ISO 11042 [26]. The sample line, filter and distribution manifolds were maintained at 433 K, with a heated pump used to deliver products to the analysis suite. Total NO_x concentrations were quantified using a heated vacuum chemiluminescence analyzer (Signal Instruments 4000VM), calibrated in the range 0-39 ppmV. Concentrations were measured hot/wet with data normalized to equivalent dry conditions prior to presentation. Sample flow was also directed to a chiller, used to reduce the molar water concentration below 1% before downstream CO and O₂ measurements were made using a combination of nondispersive infrared and paramagnetic analyzers (Signal instruments 9000MGA). These were calibrated in the respective ranges of 0-904 ppmV, and 22.52%vol.

SPECIFICATION OF EXPERIMENTAL CONDITIONS

Representative fuel fractions were taken from previous studies [4, 8], and comprised a molar composition of 65% CO, 1% H₂ and a combined diluent fraction of 34% N₂. Measurements were taken at a fixed inlet temperature of 423 ±8 K and three pressures (P₁=0.1 MPa, P₂=0.15 MPa, P₃=0.3 MPa ±2%) with net thermal power (25–75 kW) and overall flow scaled for the corresponding change in density to maintain equivalent mean nozzle exit velocities (fixed dimensionless flow parameter in an engine). A stable operating equivalence ratio was employed at $\phi = 0.65$. The lean stability limit (lean blowoff, or LBO point) was also evaluated for each experimental condition. This was defined by the ϕ that resulted in detachment from the outlet nozzle to give a lifted flame, stabilizing downstream in the quartz confinement tube with increased flow. This was obtained by incrementally increasing air supply using a digitally controlled needle valve giving steps of ~0.1 g·s⁻¹, and monitoring the flame response, until detachment was first witnessed.

This technique was shown to be repeatable, and offered reduced uncertainty at elevated pressures due to controller resolution with the increased flow.

H₂O vapor concentrations were increased to give molar reactant fractions in the range 0–0.145. Supplied concentrations were scaled in proportion with increased pressure to give equivalent changes in overall reactant composition. Thermal power restrictions with the steam supply system meant equivalent H₂O vapor fractions could not be achieved at the highest concentrations with increased pressure. Allowing for the equivalence ratio specification, full scale addition of H₂O resulted in mean velocity (\bar{u}) and bulk flow increases of 16.7% through the burner, and a 17.3% increase in Reynolds number (Re - defined by $(\bar{u} \cdot D \cdot \rho) / \mu$, where D corresponds to the burner outlet diameter, ρ – reactant density, and μ – dynamic viscosity, obtained for each mixture [27] with coefficients obtained from the NIST chemistry webbook [28]). The stable ($\Phi = 0.65$) operating parameters are summarized for each water loading and change in pressure in Table 1. Note – an additional data point was added for P₃ corresponding to 0.061 mole fraction, where H₂O supply was maximized following saturation of catalytic induced enhancement to reaction rate (see following section).

Fuel was supplied from gravimetrically blended H₂/CO and N₂ cylinder packs. Combustion air was supplied from a VSD compressor (Atlas Copco GA 45). Prior to entering the distribution pipework, the compressed air was dried using a Beko Drypoint DPRA960. The water loading at the inlet plenum was confirmed using a hygrometer (Michell Instruments S3000), returning values in the range of ~1300 to ~1600 ppmV H₂O (-19 to -17°C dew point) to give the baseline ‘dry’ condition. In addition, combustion air was analyzed using a flame ionization detector (Signal Instruments 3000HM) for hydrocarbon contamination as part of the experimental setup procedure. Concentrations were minimal, and typically measured in the range 0-1 ppmV C₃H₈ equivalent. The inlet plenum was conditioned with preheated air for up to one hour to reduce some of the effects of local heat loss.

MODELLED RESULTS

Chemical kinetics were modelled for each experimental condition using three reactors in CHEMKIN-PRO [29]: The laminar flame speed calculator uses the PREMIX program [30] to provide 1-D simulations of intermediate reaction chemistry, changes in heat release rate (HRR) and laminar flame speed (u_L). Solutions were based on an adaptive grid of 1000 points, with mixture-averaged transport properties and trace series approximation. The equilibrium tool was used to generate adiabatic flame temperatures (AFT), under conditions of constant pressure and enthalpy. Finally, the opposed flow flame reactor - utilizing the OPPDIF [30] program - was used to simulate the change in extinction strain rate (K_{Ext}) between each stable experimental condition. One-point control was used, with the premixed reactants supplied from one nozzle and N₂ from the other. An ending axial position of 1.4 cm was employed with a grid of 1000 points, adaptive mesh controls of 0.1, and a 10 K temperature step. Each simulation employed the modified Davis et al. [31] reaction mechanism (MDM) [8] comprising 14 chemical species and 38 reactions, and optimized for use with humidified syngas compositions.

H₂O addition was shown to provide two competing influences on premixed flame propagation; first a diluent effect is observed, and overall reaction rate is slowed by a reduction in AFT as shown in Fig. 3(a) (note – the experimental data points are identified by markers). For the given conditions, this was equivalent to ~250 K for the largest experimental H₂O fractions at each specified pressure. The second effect results from changes in intermediate chemistry, and the dissociative production of chain carrying species (such as HCO and OH, as shown in Fig. 4) enhancing heat release rate [4]. The catalyzing effect of these radicals on CO consumption has been shown to reduce the slow reaction (with high activation energy): $CO + O_2 \rightarrow CO_2 + O$ [4], and increase intermediate reactions such as $CO + OH \rightarrow H + CO_2$. Non-monotonic behavior in maximum net HRR is evident in Fig 3(b), with enhancement reduced and eventually reversed as molar reactant water fractions are increased beyond ~0.05-0.06. Elevated pressure is shown to provide an overall increase in max HRR, effectively reducing the catalytic influence of H₂O addition (which is consistent with other work [4]); inasmuch as there is a marginal shift in the peak to a lower water fraction, and a reduction in the proportional increase from each dry case. A similar tendency is evident with the changes in modelled u_L plotted in Fig.3(c): The H₂O-induced catalytic increase in flame speed is greater for the low pressure case; yielding a peak increase of ~73% from to the driest condition, with both overall u_L (due to density change) and the influence of H₂O reducing with increased pressure. Again, this shifts the modelled peak towards a lower H₂O fraction.

Figure 3(d) shows the modelled change in K_{Ext} with H₂O addition at each pressure, with similarities evident to change in max HRR. Although this has been shown to provide a non-monotonic trend for mixtures comprising H₂ [32], an increase in pressure over the specified range leads only to an increase in K_{Ext} for each equivalent mixture. H₂O addition was shown to provide the expected non-monotonic response in K_{Ext} ; with peaks again forming near fractions of ~0.05. However, there is again a marginal shift in peak K_{Ext} to lower H₂O fractions as pressure is increased, and the kinetic effect is diminished [33].

The OH radical was used as a marker for the chemiluminescence and PLIF techniques, and it was therefore important to analyze any potential changes in production that result from H₂O addition in detail. Figure 4 demonstrates the influence of equivalent H₂O

loadings on the 1-D spatial concentration profiles for P_1 and P_3 . H_2O addition is shown to enhance OH production and give maximum wet concentrations that are considerably higher than the dry cases, whereas an increase in pressure is shown to provide a relative reduction. Both H_2O and pressure are shown to provide spikes in OH compared to the atmospheric dry case where a relative plateau is observed, and the profiles therefore suggest strong potential differences in the signal intensities were to be expected from the diagnostics.

EXPERIMENTAL RESULTS

Reactant molar H_2O fraction was increased from 0 to 0.145 at the stable operating condition and $P_1=0.1$ MPa. The 200 image average OH* chemiluminescence response is shown in Fig. 5 - global signal for half of the 3-D flame is shown (a), together with the equivalent Abel inverted image (b), with the colormap normalized to the condition maximum intensity and flow from the bottom up. The catalytic influence of H_2O addition appears to initially reduce the zone of heat release to effectively shorten the flame, and is consistent with other work [8]. This upstream retraction of the flame provided an increase in measured burner face and lance tip temperatures, and a cooler exhaust. However, as overall reactant H_2O fraction was increased beyond 0.088, upstream retraction ceased, the overall flame brush lengthened, and all measured temperatures began to decrease. This correlates with the decrease in reactivity shown from the chemical models in Fig. 3, as the catalytic influence is saturated and quenching begins to dominate. The Reynolds numbers for each flow condition are included in Fig. 5, as increases in turbulence intensity would be expected to provide an increase in turbulent flame speed [34], and also contribute to the shortening of the heat release zone. However, the apparent flame extension suggests this enhancement has been surpassed and quenched with excessive H_2O addition. The OH* chemiluminescence of a near-equivalent ($\bar{u} = 13.5 \text{ m}\cdot\text{s}^{-1}$, $25 \text{ kW}_{\text{net}}$, $\phi = 0.66$, $T = 423 \text{ K}$, $P = 0.1 \text{ MPa}$) CH_4 /air flame has been included in the figure as a reference, to demonstrate the similarity with the H_2O -enhanced converter gas flame, compared to the differences evident with driest case. CH_4 /air u_L ($33.1 \text{ cm}\cdot\text{s}^{-1}$) was modelled using GRI-Mech 3.0 [35], suitable for application at these conditions [36], and together with Re (18.5×10^3), was within ~10% of the values for the 0.046 H_2O flame. With converter gas at 0.046 molar H_2O loading, all measured burner temperatures from the CH_4 /air flame were within 15 K, and with near-equivalent \bar{u} and Re at these conditions, the potential exists for interchangeability between fuels with minimal changes in burner design. Planar OH profiles were also obtained using the PLIF system with the 25 mm-wide laser sheet, fixed at an axial position ~5 mm downstream of the nozzle. Temporally averaged images are shown for four H_2O conditions in Fig. 6 (note – the laser sheet was supplied at an angle of ~15° to minimize internal reflections from the quartz confinement, so half-images are presented mirrored for clarity), with the plane fixed in a horizontal position at the burner centerline. The unburned reactants from the outward flow are identified by the regions of low signal intensity, with OH PLIF measured in the inner and outer recirculation zones. Higher relative OH concentrations are measured outside of the forward flow for the driest conditions, with a more uniform intensity distribution across the CRZ. As H_2O concentration rises, the highest intensities are observed along the shear layer of the CRZ, and reduce towards the center. The 1-D spatial concentration profiles in Fig. 4 suggest a sharp increase in OH for the wettest conditions followed by a fall, compared to the drier cases where the OH signal reaches a relative plateau - it therefore follows that higher relative concentrations are found closer to the reacting flow, near the axial shear layer boundary.

The influence of pressure on the flame is shown in averaged OH*chemiluminescence images for four equivalent H_2O fractions in Fig. 7, again with half the 3-D flame shown (a) above the corresponding Abel inverted image (b). With outlet velocities held constant for each relative condition, the influence of increased Reynolds number, turbulence and HRR is apparent, ostensibly shortening the flame brush. Enhancement in turbulent flame speed from increased Re [34] is therefore shown to have a greater overall effect, compared to reduction in u_L resulting from elevated pressure (Fig. 3(c)). This is caused by greater inertial forces increasing turbulence in the flow from a rise in density. An apparent reduction in flame volume from an increase in Re has also been observed in other work [37]. The enhancement of overall reaction rate provided by the limited addition of H_2O still appears to shorten the flame, although this seemingly reduces with pressure; inasmuch as there is little difference observed between the 0.024 and 0.046 flames at P_3 , compared to the marked reduction in size at P_1 . This is consistent with the modelled data which predicted a relative reduction in the catalytic influence of H_2O with increased pressure, and the effect peaking at lower concentrations. The position of the planar flame centroid was calculated from the Abel transformed images using an equivalent method employed in similar works [38], with a 70% intensity threshold used to avoid weighting from any surrounding noise. The change in axial position of the centroid downstream of the burner exit nozzle is plotted for each H_2O loading and pressure against the equivalent modelled u_L (hollow) and max HRR (shaded) in Fig. 8 (trend lines have been superimposed on the HRR data for clarity). The negative correlation between the enhancement in modelled reactivity from H_2O addition, and the change in axial flame position is evident for each pressure condition. The increase in Re resulting from enhanced bulk flow also acts to shift the flame location upstream, potentially contributing to the offset evident after the catalytic enhancement has saturated, and u_L begins to decrease.

Comparisons between the averaged OH PLIF measurements for two equivalent H_2O fractions at each pressure condition are shown in Fig. 9 - again half-images are presented mirrored for clarity. There are repeatable tendencies between each H_2O loading for all pressures: Firstly higher relative OH intensities are observed in the outer recirculation zones at dry conditions, compared to the wet results. The addition of H_2O also appears to reduce relative OH concentration inside the CRZ, giving higher intensities near the reacting

shear layer of the outward flow. These tendencies are also apparent for change in pressure; from P_1 to P_3 the CRZ shifts from a near homogenous zone, to two distinct regions, and there is lowering of the relative signal intensity in the outer recirculation zones. Again this is understandable considering the relative peaks predicted in the modelled P_3 data in Fig. 4, as products move away from the reacting flow. This greater OH consumption at pressure facilitates enhanced global CO oxidation, and helps to demonstrate how the relative dissociative influence of H_2O addition is reduced.

H_2O -induced enhancement to reactivity also provided an expected extension of the LBO stability limit [8]. As the flame compacted and H_2O fractions were increased, air flows could be driven higher resulting in globally leaner equivalence ratios. The LBO stability limit was determined for each water loading and pressure, with the corresponding equivalence ratios plotted in Fig. 10 (dotted trend lines are superimposed for clarity, and error bars represent the uncertainty in flow metering, and accuracy of the employed Coriolis meters). Air flows could be increased by up to 10-14% for all pressures when reactant H_2O fraction was 0.046, facilitating leaner operation compared to each equivalent dry condition. It should be noted that with H_2O fraction fixed, the potential exists for these limits to be marginally increased if flows were optimized for each pressure. Leaner equivalence ratios were also achieved at elevated pressure, and this is attributed to enhancements in turbulent flame speed from the increase in Re . Once the catalytic effect of H_2O addition is saturated, quenching begins to dominate, necessitating richer operation, and for the P_1 case increases beyond the original dry ϕ . There is again an ostensible tendency for the trough of each trend line to shift towards a lower H_2O fraction as the catalytic effect is reduced with an increase in pressure. Results therefore suggest that H_2O -induced catalytic enhancement to converter gas combustion would be limited with high pressure gas turbine operation, however it has been suggested that the effect is enhanced by an increase in reactant temperature [4] and further work is required to quantify and study this effect.

Emission measurements were made using the specified analytical setup: Total NO_x concentrations were measured hot and wet, and data were therefore normalized prior to presentation [23]. First, the measurement (θ_{meas}) was normalized to an equivalent dry reading (θ_{dry}) using the corresponding exhausted water fraction (X_{H_2O}) for each experimental condition (obtained from the chemical models), as shown in Eq. 1.

$$\theta_{dry} = \theta_{meas} \cdot \left(\frac{1}{1 - X_{H_2O}} \right) \quad (1)$$

The dry component was then normalized equivalent to 15% O_2 ($\theta_{dry,15\%O_2}$) dilution using the measured exhaust O_2 concentrations (θ_{O_2}), as presented in Eq. 2.

$$\theta_{dry,15\%O_2} = \theta_{dry} \cdot \left(\frac{20.9 - 15}{20.9 - \theta_{O_2}} \right) \quad (2)$$

CO was measured dry and therefore only required normalizing to the equivalent 15% O_2 condition. The normalized total NO_x and CO concentrations were obtained for each H_2O loading and pressure, and are shown in Fig. 11. The error bars represent total uncertainty in the measurement system, and comprise analyzer specifications, linearization, and accuracy in span gas certification.

There are two opposing tendencies between total NO_x and CO for elevated pressure; with the former increasing and the latter reducing for each equivalent condition. Similar trends have been witnessed in other work [39], and for CO this is attributed to lower equilibrium concentrations and faster relaxation kinetics at higher pressures [40]. The change in NO_x concentration is more dependent on burner specification and equivalence ratio [41, 42], but is likely attributed to enhanced thermal production at elevated pressure [42]. The introduction of H_2O is shown to reduce both normalized NO_x and CO concentrations to comparatively negligible levels at the highest rates of supply. This results from a drop in thermal NO_x production with reduction in adiabatic flame temperature [41], and a potential change in the water shift reaction $CO + H_2O = CO_2 + H_2$ [42]. Work undertaken by Zhao et al. [43] demonstrated the potential for kinetic increase in NO_x production from the rise in OH concentration at constant temperature, however this effect is eclipsed by thermal influences and HCN formation (significantly reduced compared to CH_4 /air flames).

From these data, power law correlations were derived from emission measurements for change in pressure at the driest conditions; with respective NO_x and CO exponents of 0.55 and -1.6. These were shown to decrease with an increase in reactant H_2O fraction, however the dataset is limited and requires further work at higher pressures. The leaner operation that was facilitated by an increase in pressure meant NO_x emissions at the LBO stability limit were similar for all pressures (10-13 ppmV $_{dry,15\%O_2}$). At molar H_2O fractions of 0.046 these concentrations were reduced by around an order of magnitude, again with similar values for all pressures (1.2-1.4 ppmV $_{dry,15\%O_2}$). CO measurements for the dry LBO flame reduced from 36 ppmV $_{dry,15\%O_2}$ at P_1 , to 3.5 ppmV $_{dry,15\%O_2}$ at P_3 , with values negligible once H_2O fractions were increased to loadings greater than 0.046.

CONCLUSIONS

Non-monotonic H₂O-induced catalytic enhancement to premixed flame behavior was observed with a representative converter gas mixture in a turbulent swirling flame. Using OH* chemiluminescence, the enhancement was initially shown to shift axial heat release location upstream toward the premixed burner nozzle as reactivity increased, and the flame brush compacted. Reactant molar H₂O fractions were elevated to a maximum of 0.145, representative of typical concentrations employed in humidified-cycle gas turbine combustion. The dissociative catalytic effect on CO oxidation was saturated as H₂O fractions were increased above 0.05, with modelled reductions in heat release rate, laminar flame speed and extinction strain rate. Consequently, the reaction was quenched and slowed, causing the flame to lengthen downstream in the flow. A comparison is also made between equivalent converter gas and CH₄ flames, with minimal difference evident in flame shape and measured temperatures for the 0.046 H₂O flame. The potential therefore exists for interchangeability between fuels with minimal changes to burner design.

The influence of pressure was investigated in the range 0.1-0.3 MPa, maintaining nozzle outlet velocities by scaling flows for the corresponding change in density. The flame was shown to compact with an increase in pressure, attributed to enhanced turbulent flame speed resulting from an increase in Reynolds number. The catalytic effect of H₂O addition was shown to reduce with increased pressure, as equivalent changes in reactant fraction made a reduced impact on the observed OH* chemiluminescence. This agreed with results obtained from chemical models. PLIF measurements were used to demonstrate enhanced OH consumption near the reaction zone, with a relative lowering of unreacted OH observed in the central and outer recirculation zones. This suggests a reduced catalytic influence of H₂O on the fuel blend in gas turbines, however further work is required to investigate the influence of reactant preheat temperature, previously shown to enhance the effect.

H₂O-induced enhancement in overall reaction rate caused a change in the operable lean stability limit; with the potential for air flow to be increased by 10-14%, for all pressures at H₂O fractions of 0.046. Increasing the water concentration further saturated the catalytic influence, quenching the flame to necessitate a reduction in air flow. Again, the effect was shown to diminish with an increase in pressure, reducing the H₂O fraction achievable before quenching began to dominate. The observed changes in flame response emphasize the potential for fluctuations in flame topology with changes to inlet or atmospheric humidity, and other premixed instabilities such as flashback.

The addition of H₂O led to a substantial reduction in both measured NO_x and CO emissions. An increase in pressure was shown to provide an increase in equivalent NO_x concentration, and a reduction to measured CO. Power law correlations were proposed for change in pressure, and showed exponents lowered with increased H₂O. However the dataset is limited, and further work is required. Emission concentrations were further reduced with the H₂O-induced shift in LBO stability limit facilitating leaner operation: NO_x concentrations dropped by an approximate order of magnitude for all pressures, with CO measurements shown to be negligible.

NOMENCLATURE

| | |
|------------------------------|------------------------------------------------------------|
| <i>AFT</i> | Adiabatic Flame Temperature, <i>K</i> |
| <i>HRR</i> | Heat Release Rate, <i>J·cm⁻¹·s⁻¹</i> |
| <i>K_{Ext}</i> | Extinction strain rate, <i>s⁻¹</i> |
| <i>LBO</i> | Lean Blow Off |
| <i>P</i> | Reactant pressure, <i>MPa</i> |
| <i>PLIF</i> | Planar Laser Induced Fluorescence |
| <i>Re</i> | Reynolds number |
| <i>T</i> | Reactant temperature, <i>K</i> |
| \bar{u} | Mean nozzle exit velocity, <i>m·s⁻¹</i> |
| <i>u_L</i> | Laminar flame speed <i>cm·s⁻¹</i> |
| <i>X_{H2O}</i> | Exhaust H ₂ O Fraction |
| ϕ | Equivalence ratio |
| θ_{meas} | Measured emission, <i>ppmV</i> |
| θ_{dry} | Dry normalized emission, <i>ppmV</i> |
| $\theta_{\text{dry,15\%O2}}$ | Normalized emission, <i>ppmV</i> |
| μ | Reactant dynamic viscosity, <i>Pa·s</i> |
| ρ | Reactant density, <i>kg·m⁻³</i> |

ACKNOWLEDGMENT

The inspiration for this work was provided by an ongoing industrial partnership with TATA Steel/EU, and supported by funding from the UK's Engineering and Physical Sciences Research Council project reference EP/M015300/1. The research was undertaken at the Cardiff University's Gas Turbine Research Centre (GTRC) with invaluable technical support from Jack Thomas and Terry Treherne.

REFERENCES

- [1] World Steel Statistics Archive, <https://www.worldsteel.org/statistics/statistics-archive.html>, accessed 02/10/2016
- [2] Remus, R., Aguado-Monsonet, M. A., Roudier, S., San, L. D., 2013, "Best Available Techniques Reference Document on the Production of Iron and Steel, Industrial Emissions Directive" 2010/75/EU, IPPC European Commission.
- [3] Das, A.K. Kumar, K. Sung, C., 2011. "Laminar flame speeds of moist syngas mixtures", *Combust. Flame*, **158**, pp 345-353.
- [4] Pugh, D.G., Crayford, A.P., Bowen, P.J., Al-Naama, M., 2016. "Parametric investigation of water loading on heavily carbonaceous syngases", *Combust. Flame*, **164**, pp 126-136.
- [5] Xie, Y. Wang, J. Xu, N. Yu, S. Zhang M., Huang, Z. 2014. "Thermal and Chemical Effects of Water Addition on Laminar Burning Velocity of Syngas", *Energ. Fuel*. **28** pp 3391-3398.
- [6] Pugh, D.G., Crayford, A.P., Bowen, P.J., O'Doherty, T. Marsh R., 2014. "Variation in Laminar Burning Velocity and Markstein Length With Water Addition for Industrially Produced Syngases", ASME Turbo Expo 2014, paper GT2014-25455.
- [7] Singh, D. Nishiie T., Tanvir S., Qiao, L. 2012. "An experimental and kinetic study of syngas/air combustion at elevated temperatures and the effect of water addition", *Fuel* **94** pp 448-456.
- [8] Pugh, D. G. Bowen P., Crayford A. Marsh R., Runyon, J. Morris, S. Giles, A., 2017 "Dissociative Influence of H₂O Vapour/Spray on Lean Blowoff and NO_x Reduction for Heavily Carbonaceous Syngas Swirling Flames" 10.1016/j.combustflame.2016.11.010
- [9] Santner, J. Dryer, F. Ju Y, 2012, "Effect of Water Content on Syngas Combustion at Elevated Pressure", 50th AIAA Aerospace Sciences Meeting (2012), paper AIAA 2012-0163.
- [10] Donohoe, N. Heufer, K. A. Aul, C. J. Petersen, E. L. Bourque, G. Gordon, R. Curran, H. J. 2015. "Influence of steam dilution on the ignition of hydrogen, syngas and natural gas blends at elevated pressures", *Combust. Flame*, **162**, pp 1126-1135.
- [11] Kéromnès, A. Metcalfe, W. K. Heufer, K. A. Donohoe, N. Das, A. K. Sung, J. Herzler, C. Naumann, P. Griebel, O. Mathieu, M. C. Krejci, E. L. Petersen, C. Pitz, W. J. Curran, H. J. 2013. "An experimental and detailed chemical kinetic modeling study of hydrogen and syngas mixture oxidation at elevated pressures", *Combust. Flame*, **160**, pp 995-1011.
- [12] Krejci, M. C. Mathieu, O. Vissotski, A. J. Ravi, S. Sikes, T. G. Petersen, E. L. Kéromnès, A. Metcalfe, W. Curran H. J. 2013 "Laminar Flame Speed and Ignition Delay Time Data for the Kinetic Modeling of Hydrogen and Syngas Fuel Blends". ASME. J. Eng. Gas Turbines Power **135**.
- [13] Combined Cycle Systems for Near-Zero Emission Power Generation – Chapter 5
- [14] Chigier, N.A. Beer, J.M. 1964. "The Flow Region Near the Nozzle in Double Concentric Jets", *J. Basic Eng.* **4** pp 797–804.
- [15] Sheen, H.J. Chen, W.J. Jeng, S.Y. Huang T.L., 1996 "Correlation of swirl number for a radial-type swirl generator", *Exp. Therm. Fluid Sci.* **12** pp 444–451.
- [16] Cabot G., Vauchelles D., Taupin, B. Boukhalfa, A. 2004. "Experimental study of lean premixed turbulent combustion in a scale gas turbine chamber", *Exp. Therm. Fluid Sci.* **28** pp 683-690.
- [17] Panoutsos C.S., Hardalupas, Y. Taylor A.M.K.P., 2009. "Numerical evaluation of equivalence ratio measurement using OH* and CH* chemiluminescence in premixed and non-premixed methane-air flames", *Combust. Flame* **156** pp 273-291.
- [18] Lauer, M. Sattelmayer, T. 2008 "Heat Release Calculation in a Turbulent Swirl Flame from Laser and Chemiluminescence Measurements, 14th International Symposium on Applications of Laser Techniques to Fluid Mechanics".
- [19] Marsh R., Runyon J., Giles A., Morris S., Pugh, D.G. Valera-Medina, A. Bowen, P.J. 2016 "Premixed Methane oxycombustion in Nitrogen and Carbon Dioxide atmospheres: Measurement of operating limits, flame location and emissions", *Proc. Combust. Inst.* (2016).
- [20] Taamallah, S. Shanbhogue, S.J. Ghoniem, A.F. 2016. "Turbulent flame stabilization modes in premixed swirl combustion: Physical mechanism and Karlovitz number-based criterion", *Combust. Flame* **166** pp 19-33.
- [21] Killer, C. Abel Inversion Algorithm, <http://www.mathworks.com/matlabcentral/fileexchange/43639-abel-inversion-algorithm>, 2013, accessed 01/12/2015.
- [22] Shanbhogue, S.J. Sanusi Y.S., Taamallah S., Habib M.A., Mokheimer, E.M.A. Ghoniem, A.F. 2016 "Flame macrostructures, combustion instability and extinction strain scaling in swirl-stabilized premixed CH₄/H₂ combustion", *Combust. Flame* **163** pp 494-507.
- [23] Runyon, J. Marsh, R. Sevcenco Y., Pugh D., Morris, S. 2015 "Development and commissioning of a chemiluminescence imaging system for an optically-accessible high-pressure generic swirl burner", 7th European Combustion Meeting, paper P3-29.
- [24] Krishna, S. Ravikrishna R., 2015. "Quantitative OH Planar Laser Induced Fluorescence Diagnostics of Syngas and Methane Combustion in a Cavity Combustor", *Combust. Sci. Technol.* **187** pp 1661-1682.
- [25] Stopper, U. Meier, W. Sadanandan, R. Stöhr M., Aigner, M. Bulat, G. 2103 "Experimental study of industrial gas turbine flames including quantification of pressure influence on flow field, fuel/air premixing and flame shape", *Combust. Flame* **160** pp 2103-2118.
- [26] British Standard ISO 11042-1:1996, Gas turbines. Exhaust gas emission. Measurement and evaluation, British Standards Institution, U.K., 1996.
- [27] Herning, L. and Zipperer. 1936 *Gas and Wasserfach* **79** pp 49.
- [28] NIST chemistry web-book, <http://webbook.nist.gov/chemistry/>, Accessed 10/10/2016.
- [29] CHEMKIN-PRO 15131, Reaction Design: San Diego, 2009.
- [30] Kee, R.J. Rupley F.M., Miller, J.A. Coltrin, M.E. Grear J.F., Meeks, E. Moffat H.K., Lutz, A.E. Dixon-Lewis G., Smooke M.D., Warnatz, J. Evans G.H., Larson, R.S. Mitchell, R.E., Petzold L.R., Reynolds W.C., Caracotsios M., Stewart W.E., Glarborg P., Wang C., Adigun O., CHEMKIN Collection Release 3.6, Reaction Design, San Deigo, USA, 2000.
- [31] Davis, S.G. Joshi A.V., Wang, H. Egolfopoulos F., 2005. "An optimized kinetic model of H₂/CO combustion", *Proc. Combust. Inst.* **30** pp 1283-1292.
- [32] Niemann, U., Seshadri, K., Williams, F., 2013, "Effect of pressure on structure and extinction of near-limit hydrogen counterflow diffusion flames," *Proc. Combust. Inst.*, **34**, pp. 881-886.
- [33] C.K Law, 2006. *Combustion Physics*, Cambridge University Press, U.K.,
- [34] Flohr, P. Pitsch, H. 2000, "A turbulent flame speed closure model for LES of industrial burner flows" Center for Turbulence Research Proceedings of the Summer Program 2000
- [35] Bowman C., Frenklach M., Gardiner, W., Smith, G., 1999, "The 'GRIMech 3.0' chemical kinetic mechanism." www.me.berkeley.edu/grimech.
- [36] Hu, E. Li, X. Meng, X. Chen, Y. Cheng, Y. Xie, Y. Huang, Z. 2015. "Laminar flame speeds and ignition delay times of methane-air mixtures at elevated temperatures and pressures", *Fuel*, **158**, pp 1-10.

- [37] Carlsson, H. Nordström, E. Bohlin, A. Wu, Y. Zhou, B. Li, Z. Aldén, M. Bengtsson P., Bai, X. 2015. "Numerical and experimental study of flame propagation and quenching of lean premixed turbulent low swirl flames at different Reynolds numbers" *Combust. Flame*, **162** pp 2582-2591.
- [38] Han, Z. and Hochgreb, S., 2015, "The response of stratified swirling flames to acoustic forcing: Experiments and comparison to model," *Proc. Combust. Inst.*, 35(3), pp. 3309-3315.
- [39] Kobayashi, H. Yata, S. Ichikawa Y., Ogami, Y. 2009, "Dilution effects of superheated water vapor on turbulent premixed flames at high pressure and high temperature", *Proc. Combust. Inst.* **32** pp 2607-2614.
- [40] Amato, A. Hudak, B. D'Souza P. D'Carlo, P. Noble, D. Scarborough, D. Seitzman, J. Lieuwen, T. 2011 "Measurements and analysis of CO and O2 emissions in CH4/CO2/O2 flames" *Proc. Combust. Inst.* **33** pp 3399-3405
- [41] Furuhashi T., Kawata, T. Mizukoshi N., Arai M., 2010. "Effect of steam addition pathways on NO reduction characteristics in a can-type spray combustor", *Fuel* **89** (2010) 3119-3126.
- [42] Biagioli, F. Güthe, F. 2007. "Effect of pressure and fuel-air unmixedness on NOx emissions from industrial gas turbine burners", *Combust. Flame*, **151**, pp 274-288
- [43] Zhao, D. Yamashita, H. Kitagawa K., Arai, N. Furuhashi T., 2002. "Behavior and effect on NOx formation of OH radical in methane-air diffusion flame with steam addition", *Combust. Flame* **130** pp 352-360.

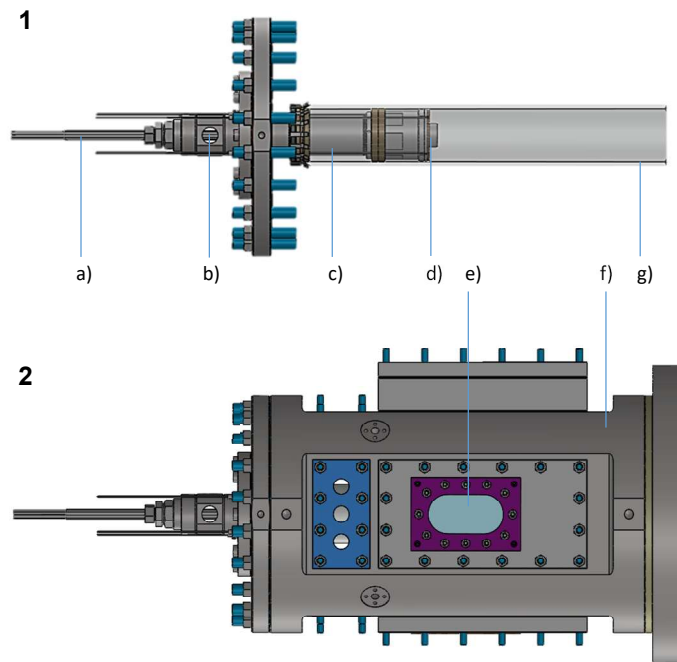


Figure 1. SWIRL BURNER ASSEMBLY SCHEMATIC (1) AND PRESSURE CASING WITH OPTICAL ACCESS (2).

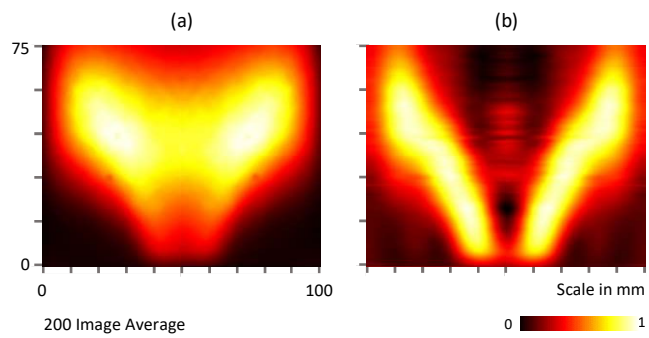


Figure 2. RAW CHEMILUMINESCENCE IMAGE OF AN AXISYMMETRIC SAMPLE FLAME (a) AND THE EQUIVALENT ABEL DECONVOLUTED IMAGE (b).

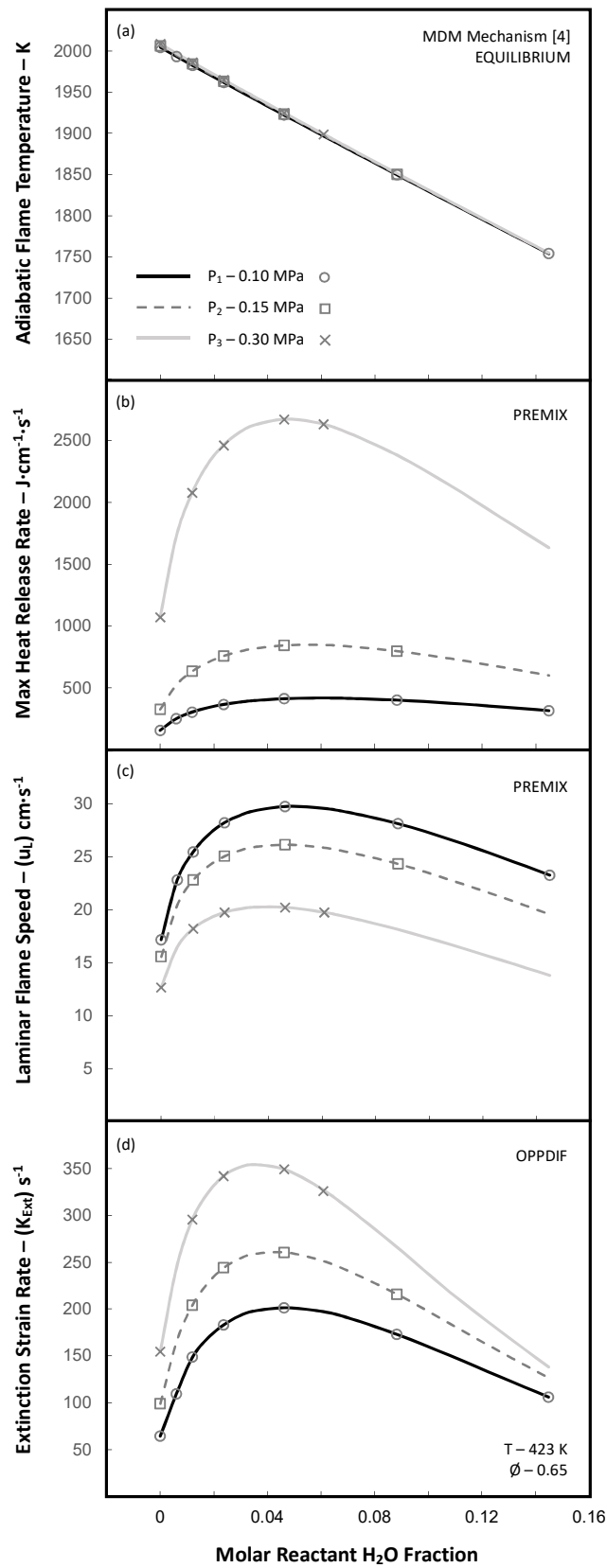


Figure 3. MODELLED CHANGES IN; AFT (a) MAXIMUM HRR (b) u_L (c) AND K_{Ext} (d) FOR EACH STABLE OPTATING CONDITION. EXPERIMENTAL POINTS ARE IDENTIFIED AS MARKERS.

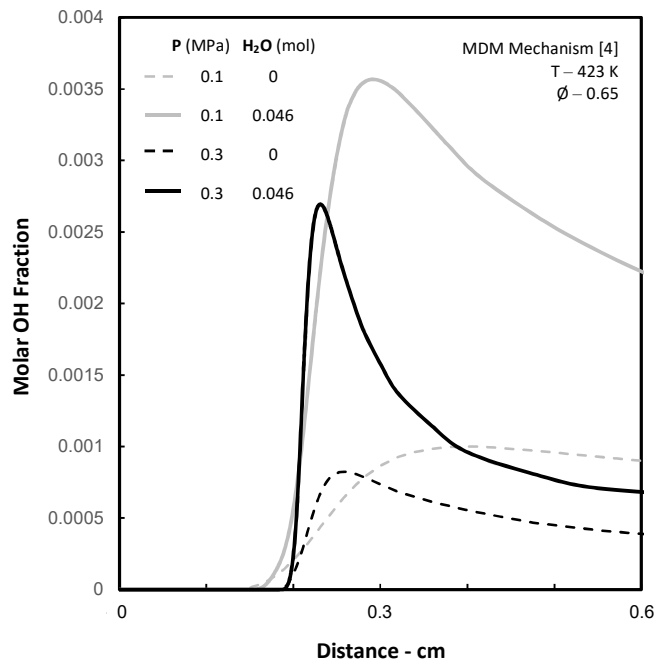


Figure 4. 1-D OH SPATIAL CONCENTRATION PROFILES FOR P₁ AND P₃ AND TWO EQUIVALENT WATER LOADINGS.

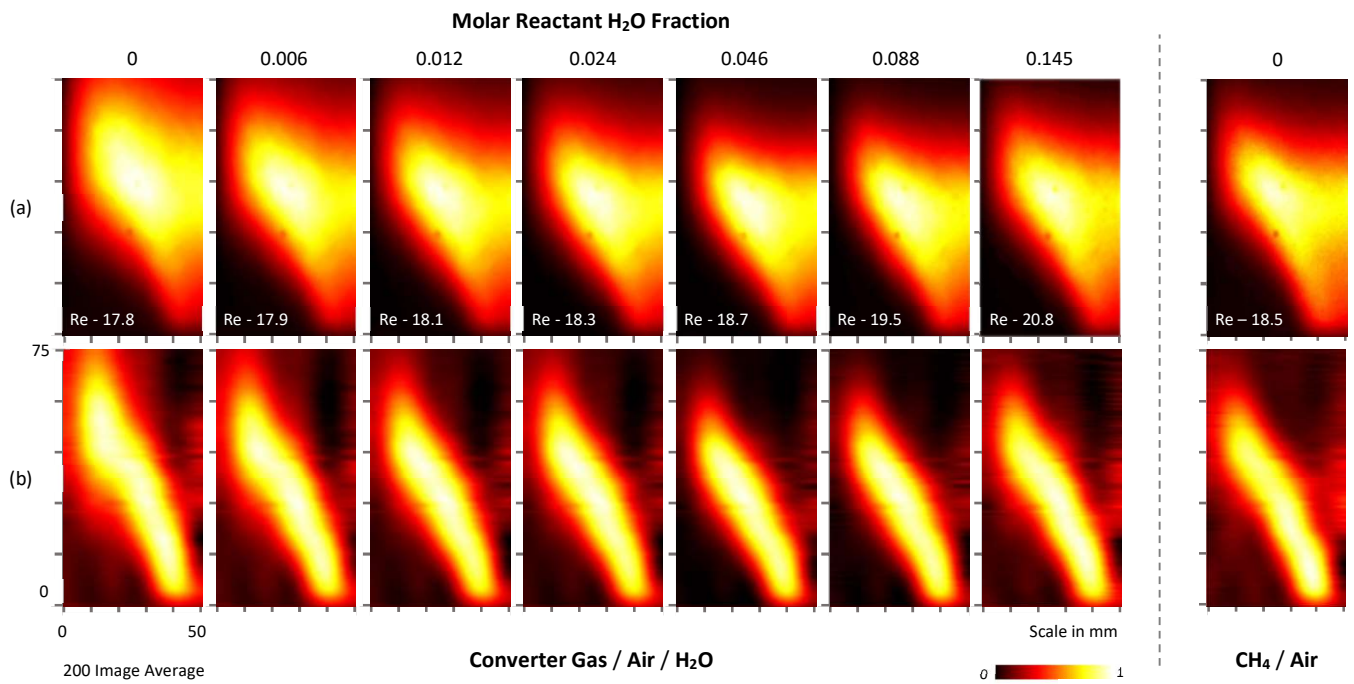


Figure 5. AVERAGE OH* CHEMILUMINESCENCE IMAGES FOR CONVERTER GAS AND CH₄ FLAMES (a), AND EQUIVALENT ABEL TRANSFORMED IMAGES (b) AT $\phi=0.65$ WITH INCREASING LEVELS OF H₂O ADDITION ($Re \times 10^3$).

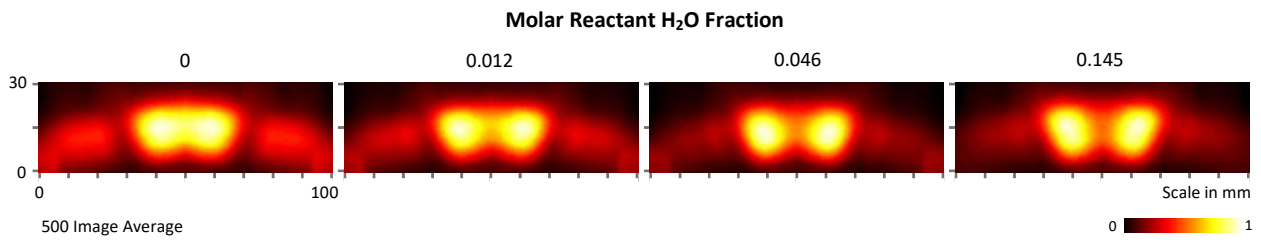


Figure 6. AVERAGE MIRRORED OH PLIF INTENSITIES FOR $\phi=0.65$ WITH INCREASING LEVELS OF H₂O ADDITION.

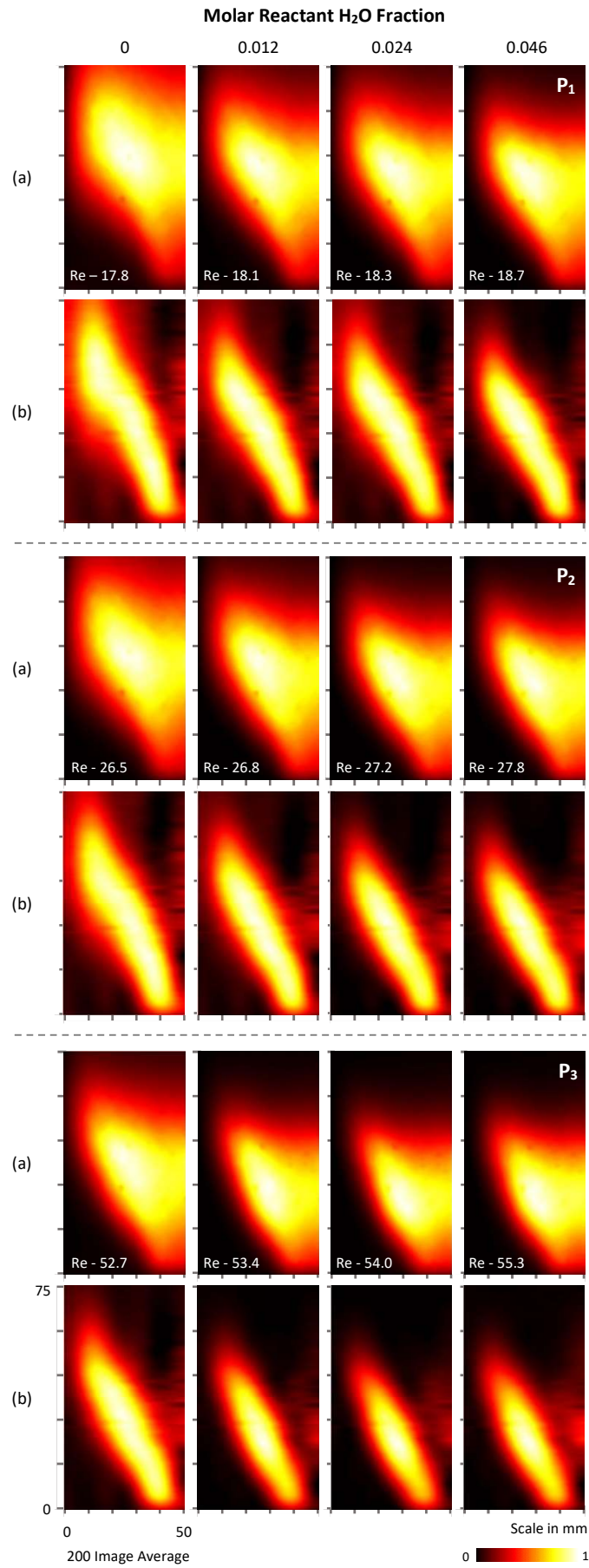


Figure 7. AVERAGE OH* CHEMILUMINESCENCE (GLOBAL (a), ABEL (b)) WITH EQUIVALENT H₂O ADDITION FOR P₁, P₂, AND P₃ (Re x10³).

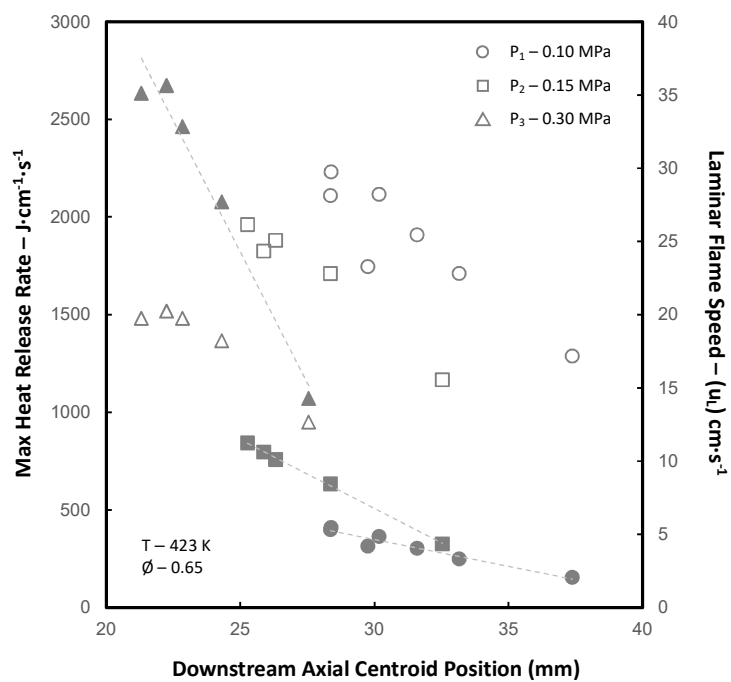


Figure 8. CHANGE IN AXIAL FLAME CENTROID LOCATION AGAINST MODELLED u_L (HOLLOW) AND MAX HRR (SHADED).

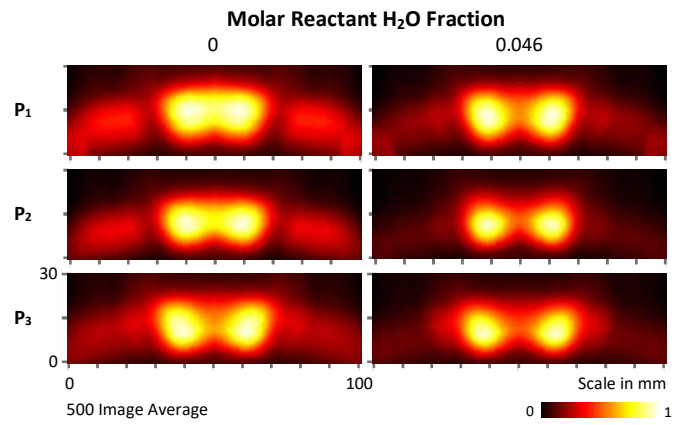


Figure 9. MIRRORED AVERAGE OH PLIF INTENSITIES FOR P₁, P₂, AND P₃ WITH EQUIVALENT LEVELS OF H₂O ADDITION.

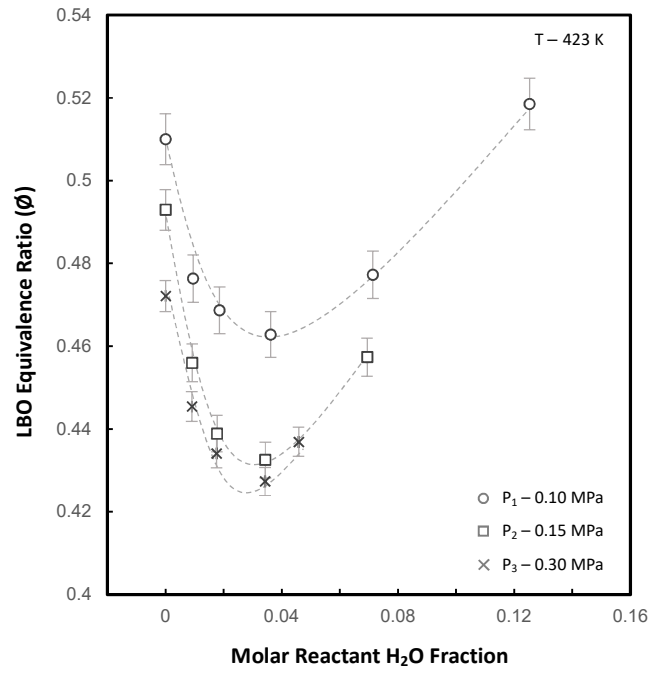


Figure 10. CHANGE IN LBO EQUIVALENCE RATIO FOR ALL EXPERIMENTAL CONFIGURATIONS.

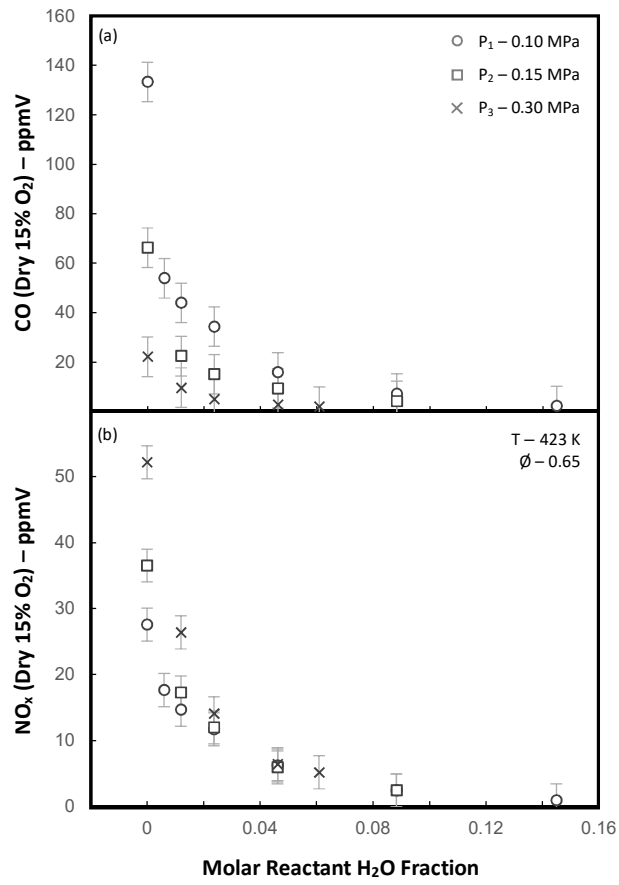


Figure 11. CHANGE IN NORMALISED CO (a) AND NO_x (b) CONCENTRATIONS FOR $\phi = 0.65$ ACROSS ALL CONDITIONS.

Table 1. OPERATING PARAMETERS FOR STABLE $\phi = 0.65$ WITH CHANGE IN PRESSURE AND REACTANT H₂O FRACTION.

| Reactant Water Fraction (<i>mol</i>) | Pressure range (<i>MPa</i>) | Mean Velocity (\bar{u}) (<i>m·s⁻¹</i>) | Reynolds Number (Re) (<i>x 10³</i>) | Mass Flow Air (<i>g·s⁻¹</i>) | Mass Flow Fuel (<i>g·s⁻¹</i>) | Mass Flow Water (<i>g·s⁻¹</i>) | Net Thermal Power (LHV) (<i>kW</i>) |
|--------------------------------------------------|-----------------------------------------|----------------------------------------------------------------------------|------------------------------------------------------------|-----------------------------------------------------|------------------------------------------------------|-------------------------------------------------------|-------------------------------------------------|
| 0.000 | 0.1 - 0.3 | 12.92 | 17.8 - 52.7 | 9.4 - 28 | 3.74 - 11.2 | 0 | 25 - 75 |
| 0.006 | 0.1 | 13.03 | 17.9 | 9.4 | 3.74 | 0.05 | 25 |
| 0.012 | 0.1 - 0.3 | 13.12 | 18.1 - 53.4 | 9.4 - 28 | 3.74 - 11.2 | 0.1 - 0.3 | 25 - 75 |
| 0.024 | 0.1 - 0.3 | 13.27 | 18.3 - 54 | 9.4 - 28 | 3.74 - 11.2 | 0.2 - 0.6 | 25 - 75 |
| 0.046 | 0.1 - 0.3 | 13.54 | 18.7 - 55.3 | 9.4 - 28 | 3.74 - 11.2 | 0.4 - 1.2 | 25 - 75 |
| 0.061 | 0.3 | 13.62 | 56.3 | 28 | 11.2 | 1.6 | 75 |
| 0.088 | 0.1 - 0.15 | 14.11 | 19.5 - 29.2 | 9.4 - 28 | 3.74 - 5.59 | 0.8 - 1.2 | 25 - 50 |
| 0.145 | 0.1 | 15.08 | 20.8 | 9.4 | 3.74 | 1.4 | 25 |

